

# First-principles study of structural, elastic, and bonding properties of pyrochlores

J. M. Pruneda<sup>1,2</sup> and Emilio Artacho<sup>1,3</sup>

<sup>1</sup>*Department of Earth Sciences, University of Cambridge Downing Street, Cambridge, CB2 3EQ, United Kingdom*

<sup>2</sup>*Institut de Ciència de Materials de Barcelona (CSIC), Spain.*

<sup>3</sup>*Donostia International Physics Center (DIPC),*

*Paseo Manuel de Lardizabal 4, 20018 Donostia-San Sebastián, Spain*

(Dated: March 23, 2022)

Density Functional Theory calculations have been performed to obtain lattice parameters, elastic constants, and electronic properties of ideal pyrochlores with the composition  $A_2B_2O_7$  (where  $A=La,Y$  and  $B=Ti,Sn,Hf,Zr$ ). Some thermal properties are also inferred from the elastic properties. A decrease of the sound velocity (and thus, of the Debye temperature) with the atomic mass of the B ion is observed. Static and dynamical atomic charges are obtained to quantify the degree of covalency/ionicity. A large anomalous contribution to the dynamical charge is observed for Hf, Zr, and specially for Ti. It is attributed to the hybridization between occupied  $2p$  states of oxygen and unoccupied  $d$  states of the B cation. The analysis based on Mulliken population and deformation charge integrated in the Voronoi polyhedra indicates that the ionicity of these pyrochlores increases in the order  $Sn-Ti-Hf-Zr$ . The charge deformation contour plots support this assignment.

PACS numbers: 71.20.-b, 62.20.-x, 65.40.-b, 91.60.Ki

## I. INTRODUCTION

Materials with the pyrochlore ( $A_2B_2O_7$ ) lattice structure have unique properties that make them ideal candidates for applications ranging from high-permittivity dielectrics<sup>1</sup>, to ceramic thermal barrier coatings (TBC)<sup>2</sup>, potential solid electrolytes in solid-oxide fuel cells<sup>3</sup>, or immobilization hosts of actinides in nuclear waste<sup>4</sup>. Many studies have tried to optimize the pyrochlore composition to obtain the most desirable properties for a particular application. One has to achieve maximum efficiency in a special property (high dielectric constant, low thermal conductivity, low migration energies, etc.), but at the same time satisfy other requirements such as physical stability, chemical or thermal compatibility with other materials involved in the design, etc. In many cases, no experimental information is available, or if there is information there is no agreement between different experiments, a consequence of the difficulties in growing pure samples.

Therefore, simulations have become an ideal tool for systematic investigations of various properties as a function of the chemical composition<sup>5,6,7,9,10</sup>. Most of the atomistic simulations studies are based in classical potential methods, where the interatomic interactions are parametrized with effective potentials fitted to reproduce experimentally known data, as the unit cell dimensions of a variety of oxide pyrochlores. The complexity of the chemical elements involved (mostly transition metals and rare earths) makes desirable the use of *ab initio* calculations, but the large size of the unit cell in pyrochlores (88 atoms) had restricted the application of this technique.

The limitations of these classical models have recently been pointed out by Panero et. al.<sup>11</sup> in the study of the energetics of cation-antisite defects. The stability of pyrochlores and the resistance to amorphization by irradiation has been correlated with the propensity of the

ions to create these point defects<sup>5</sup>. With classical models, the defect-formation energies show a dependence on the cationic radius: compounds with similar radii for A and B are more radiation resistant than compounds with very dissimilar radii, that show greater susceptibility to amorphization. The effect of the B cation radius seems to be more important than the effect of the A cation. Nevertheless, density functional calculations<sup>11</sup> have shown that the defect formation energies are not simple functions of the cationic radius, and a significant influence of the electronic configuration of the A and B cations is observed.

It is now believed that the radiation response cannot be described exclusively in terms of the cationic radius ratio and the defect formation energies, and that the bond-type must be considered.<sup>4,12,13,14,15</sup> It has been suggested that the resistance of materials to amorphization of a complex non-metallic compound is determined by a competition between short-range covalent interactions, and long-range ionic forces.<sup>15,16</sup> This picture is based on experimental evidences for more than 100 different materials, with very different chemical and structural compositions. Unfortunately, it is not easy to quantify the covalency/ionicity and relate this to radiation resistance, specially when the *topological freedom* of the lattice structure can play an important role<sup>17</sup>.

The broad range of chemical properties that can be obtained changing the composition of A- and B-site cations in the pyrochlore structure, makes them good testing systems to study the relationship between electronic structure and resistance to amorphization by radiation damage. Compounds with strong ionic character, like the zirconates ( $A_2Zr_2O_7$ ) are known to be more resistant to radiation to clearly covalent stannates ( $A_2Sn_2O_7$ ). Experiments with  $Gd_2(Zr_xTi_{1-x})_2O_7$  show that the radiation resistance increases with increasing Zr-content, a clear indication of the effect of the electronic structure.

Here we present first principles calculations of two families of pyrochlores:  $\text{La}_2\text{B}_2\text{O}_7$  and  $\text{Y}_2\text{B}_2\text{O}_7$ , with  $\text{B}=\text{Ti}$ ,  $\text{Zr}$ ,  $\text{Sn}$  or  $\text{Hf}$  with very different bonding properties. The structural properties and elastic constants are compared with available experimental information<sup>18</sup>, as well as with data obtained with classical atomic models. The structural information obtained with these *ab initio* calculations can be used to improve the classical interatomic potentials available.

We will discuss the electronic properties of the different compounds and try to quantify the ionicity/covalency of the different bonds. Static and dynamical charges are frequently used to characterize the nature of bonds in molecules and solids. Static charges associated to an isolated atom are intuitive but ill-defined quantities. Dynamical charges, on the other side, are less intuitive, but appear as a more fundamental quantity. These dynamical charges are very sensitive to the structural properties, but also to partial hybridization between occupied and unoccupied states,<sup>19</sup> and hence they can give valuable information on the nature of the atomic bonds.

The paper is organized as follows. In Sec. II, we will describe the structural properties of the pyrochlores studied. Section III analyses the electronic properties of the different bonds, in terms of static and dynamical charges, charge density distribution, and decomposition of the partial density of states (PDOS). In Sec. IV, a discussion of our results is presented, and experimental evidences for radiation resistance are examined. Finally, conclusions are given in Sec. V.

## II. STRUCTURAL PROPERTIES

The ideal pyrochlore structure is isometric with space group  $\text{Fd}\bar{3}\text{m}$ , and eight molecules in the unit cell. It can be visualized in a variety of ways<sup>20</sup>, but is often considered as an ordered defect fluorite structure. The A and B metal cations occupy the 16d ( $\frac{1}{2}, \frac{1}{2}, \frac{1}{2}$ ) and 16c (0, 0, 0) sites respectively, and the oxygens are in the 48f ( $x, \frac{1}{8}, \frac{1}{8}$ ) and 8b ( $\frac{3}{8}, \frac{3}{8}, \frac{3}{8}$ ) positions. The anion sublattice could be completed adding the missing oxygen in the 8a site to form the fluorite structure. The system is completely described in terms of the lattice size  $a$ , and  $x$  parameter defining the position of the  $\text{O}_{48\text{f}}$ . Geometrically, the smaller  $\text{B}^{+4}$  cation is surrounded by six  $\text{O}_{48\text{f}}$  in a distorted octahedron, and the large  $\text{A}^{+3}$  cation is in a distorted cubic polyhedron formed by two  $\text{O}_{8\text{b}}$  and six  $\text{O}_{48\text{f}}$ . The 48f oxygen is coordinated to two A and two B sites, and the 8b oxygen is inside a tetrahedron formed by  $\text{A}^{+3}$  cations.

We have used a variable cell conjugate-gradient minimization of the energy following the forces and stresses to obtain a relaxed minimum-energy structure for each of the studied systems. First principles calculations are performed with the self-consistent SIESTA method,<sup>21</sup> using Density Functional Theory (DFT)<sup>22</sup> within the Local Density Approximation (LDA).<sup>23</sup> Norm-conserving

pseudopotentials<sup>24</sup> in the Kleinman-Bylander form<sup>25</sup> are generated with the following atomic valence configurations:  $\text{Ti}(3\text{s}^2, 3\text{p}^6, 3\text{d}^2, 4\text{s}^2)$ ,  $\text{Y}(5\text{s}^2, 4\text{p}^6, 4\text{d}^1)$ ,  $\text{Zr}(4\text{s}^2, 4\text{p}^6, 4\text{d}^2, 5\text{s}^2)$ ,  $\text{Sn}(5\text{s}^2, 5\text{p}^2)$ ,  $\text{La}(5\text{s}^2, 5\text{p}^6, 5\text{d}^1, 6\text{s}^2)$ , and  $\text{Hf}(6\text{s}^1, 5\text{d}^3)$ . These, include nonlinear partial-core corrections<sup>26</sup> and/or semicore states to account for the large overlap between core and valence states. We used a single- $\zeta$  basis set for the semicore states and double- $\zeta$  plus polarization for the valence states. The charge density is projected on a real space uniform grid with an equivalent plane-wave cutoff of 280 Ry, to calculate the exchange-correlation and Hartree matrix elements in the Hamiltonian. Brillouin zone summations are carried out with a  $3\times 3\times 3$  Monkhorst-Pack k-point mesh.

### A. Structural parameters

The relaxed lattice sizes, and  $x$  parameters are given in Table I. In general, the calculated LDA lattice parameters are underestimated, but the agreement with available experimental data<sup>7,8,13,27</sup> is better than  $\sim 1\%$ . There is also good agreement with other first principles calculations.<sup>10,11</sup> However small deviations exist when  $x$  is compared to the values calculated using classical models. These calculations predict an increase in  $x$  with the B cation radius<sup>28</sup>. We do not observe this clear trend, although the differences appear mainly for the stannates, where the covalent character of tin makes the definition of ionic radii, at least, questionable. To further validate the calculated structures for these pyrochlores, we show in Tab.I the most relevant bond distances and angles. The agreement again is remarkable with deviations to experimental values not bigger than  $\sim 2\%$ .

### B. Elastic constants

The linear elastic constants can be obtained from first principles with the derivatives of the stress as a function of a properly chosen lattice distortion  $\delta$  parametrizing the strain.<sup>29</sup> For a cubic structure, the number of independent elastic constants is reduced to three:  $c_{11}$ ,  $c_{12}$  and  $c_{44}$ . They can be obtained through volume compression, tetragonal and trigonal strains:<sup>30</sup>

$$\begin{aligned} \epsilon_{cmp} &= \frac{1}{3} \begin{pmatrix} \delta & 0 & 0 \\ 0 & \delta & 0 \\ 0 & 0 & \delta \end{pmatrix} \longrightarrow \frac{\partial \sigma_{11}}{\partial \delta} = B = \frac{c_{11} + 2c_{12}}{3} \\ \epsilon_{tet} &= \frac{1}{2} \begin{pmatrix} -\delta & 0 & 0 \\ 0 & -\delta & 0 \\ 0 & 0 & 2\delta \end{pmatrix} \longrightarrow \frac{\partial \sigma_{11}}{\partial \delta} = C' = \frac{1}{2}(c_{11} - c_{12}) \\ \epsilon_{tri} &= \begin{pmatrix} \delta^2 & \delta & \delta \\ \delta & \delta^2 & \delta \\ \delta & \delta & \delta^2 \end{pmatrix} \longrightarrow \frac{\partial \sigma_{21}}{\partial \delta} = 2c_{44} \end{aligned}$$

where  $B$  and  $C'$  are the bulk modulus and the shear modulus. When the applied strain reduces the symmetry of the crystal structure adding new internal degrees of freedom for the atomic positions, these have to be fully relaxed to obtain the elastic constants. In Table II we show the results for the elastic constants and bulk modulus, both for the distorted cells without geometry relaxations ( $c_{ij}^0$ ), and for those structures resulting in internal atomic relaxations. It can be seen that the relaxation has a strong effect on the elastic constants, specially for  $c_{44}$  that is softened up to a 40% when the atomic positions are optimized. To the best of our knowledge, no experimental data is available for the pyrochlores studied in this work. It has to be considered that the values presented in Table II were obtained at  $T = 0\text{K}$ , and that temperature effects generally reduce the values for the elastic constants. Consequently, we expect the experimental values at room temperature to be smaller than the values presented here.

From the elastic constants we can obtain some information on the thermal properties of the pyrochlores. The

TABLE I: Calculated lattice parameters for  $A_2B_2O_7$  pyrochlores, compared to experimental and calculated values. Th.A shows results for other first principles simulations. Th.B shows results obtained with empirical potentials.

	a	x	$d_{A-O_{8a}}$	$d_{A-O_{48f}}$	$d_{B-O_{48f}}$	$\widehat{BOB}$
<b><math>La_2Sn_2O_7</math></b>						
<i>This work</i>	10.744	0.3341	2.33	2.61	2.10	129.1
Exp.[27]	10.703	0.329	2.32	2.63	2.07	131.6
Th.B[7]		0.324				
<b><math>La_2Zr_2O_7</math></b>						
<i>This work</i>	10.724	0.3314	2.32	2.62	2.09	130.5
Exp.[8]	10.737	0.331				
Exp.[7]	10.805	0.333	2.34	2.64	2.10	130.6
Th.A[10]	10.986	0.330				
Th.B[7]		0.326				
<b><math>La_2Hf_2O_7</math></b>						
<i>This work</i>	10.673	0.3298	2.31	2.62	2.07	131.4
Exp.[8]	10.750	0.331				
<b><math>La_2Ti_2O_7</math></b>						
<i>This work</i>	10.366	0.3227	2.24	2.59	1.98	135.6
Th.A[10]	10.541	0.323	2.28	2.63	2.02	135.1
<b><math>Y_2Sn_2O_7</math></b>						
<i>This work</i>	10.348	0.3437	2.24	2.44	2.07	124.1
Exp.[27]	10.372	0.337	2.25	2.49	2.04	127.6
Th.A[11]	10.329	0.338				
Th.B[7]		0.329				
<b><math>Y_2Zr_2O_7</math></b>						
<i>This work</i>	10.335	0.3417	2.24	2.45	2.06	125.1
Th.A[11]	10.463	0.342	2.26	2.48	2.08	125.0
<b><math>Y_2Hf_2O_7</math></b>						
<i>This work</i>	10.300	0.3399	2.23	2.46	2.04	126.1
<b><math>Y_2Ti_2O_7</math></b>						
<i>This work</i>	9.974	0.3321	2.16	2.43	1.94	130.2
Exp.[13]	10.100	0.330	2.18	2.46	1.96	131.3
Th.A[11]	10.049	0.329				
Th.B[7]		0.325				

TABLE II: Calculated elastic constants (in GPa) for  $A_2B_2O_7$  pyrochlores.

	$c_{11}^0$	$c_{12}^0$	$c_{44}^0$	$B^0$	$c_{11}$	$c_{12}$	$c_{44}$	$B$
$La_2Ti_2O_7$	336	148	309	211	241	196	213	211
$Y_2Ti_2O_7$	388	160	318	236	381	153	241	229
$La_2Zr_2O_7$	313	164	305	213	290	156	200	200
$Y_2Zr_2O_7$	394	170	312	245	351	163	198	225
$La_2Hf_2O_7$	339	166	327	224	322	149	214	207
$Y_2Hf_2O_7$	403	191	343	262	379	167	221	238
$La_2Sn_2O_7$	295	131	280	185	295	131	183	185
$Y_2Sn_2O_7$	354	141	289	212	348	140	202	209

longitudinal and transverse acoustic velocities (along the [100] direction) are estimated with  $v_l = \sqrt{c_{11}/\rho}$  and  $v_t = \sqrt{c_{44}/\rho}$ , where  $\rho$  is the mass density of the material.<sup>31</sup> We can then define the mean sound velocity as:

$$\frac{1}{v^3} = \frac{1}{3} \left( \frac{1}{v_l^3} + \frac{2}{v_t^3} \right)$$

We observe that the resulting velocities (shown in Fig.1) decrease with the atomic mass of the B cation, and also with the mass of A. We do not observe a clear trend with the cationic radii. These velocities can also be used to calculate Debye's characteristic temperature<sup>32</sup>  $\Theta_D = (h\nu/k_B)(3N_o/4\pi V)^{1/3}$ , for a solid with  $N_o$  atoms in the volume  $V$ , and where  $h$  is Plank's constant,  $k_B$  is Boltzmann constant (see inset in Fig.1).

### III. ELECTRONIC PROPERTIES

The concept of *atomic charge* is widely used in chemistry as well as in solid state physics. Unfortunately, it

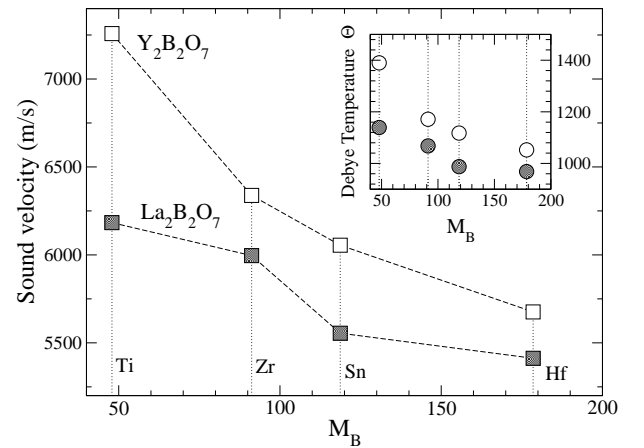


FIG. 1: Calculated mean sound velocity as a function of the atomic mass of the B site for the two families of pyrochlores studied:  $Y_2B_2O_7$  (empty symbols) and  $La_2B_2O_7$  (filled symbols). The Debye temperatures  $\Theta$  (in K) are shown in the inset.

is not a well defined concept. Many different definitions have been proposed and there is not a general agreement in how to partition the electronic charge density around the atoms and quantify the atomic charge. Behind this technical problem lies a more fundamental one: the quantification of the covalency/ionicity of chemical bonds. Here we present the results obtained with several definitions of atomic charges, in order to characterize the nature of the different bonds in the family of pyrochlores.

### A. Dynamical charges

The so called *dynamical charges* (or Born charges) are defined in terms of the change of the polarization created when an atom is displaced from its equilibrium position. They have been used to characterize the ionicity/covalency in ferroelectric perovskites.<sup>33</sup> The tensorial definition is:

$$Z_{i,\alpha\beta}^* = \Omega_0 \frac{\partial P_\beta}{\partial u_{i,\alpha}} \quad (1)$$

where  $P_\beta$  is the  $\beta$  component of the macroscopic polarization induced per unit cell when the atom  $i$  is displaced in the direction  $u_\alpha$ , and  $\Omega_0$  is the unit cell volume.

The Born effective charges for the four inequivalent lattice points are shown in Table III. The charge neutrality sum rule ( $\sum Z^* = 0$ ) is frequently used to benchmark the accuracy of the calculation, and in our case is fulfilled to within  $0.04e$ . The symmetry of the A and B sites allow for a decomposition of the Born charge tensors into two independent eigenvalues, one for displacements pointing in the direction  $[111]$  and the others (degenerate) for displacements in the orthogonal plane. For the A site, the highest eigencharge corresponds to the  $[111]$  direction, due to the presence of the  $O_{8b}$  along this axis. On the other side, the  $[111]$  gives the smallest eigencharge because the  $O_{8a}$  site is unoccupied in pyrochlores. Small deviations from the two-fold degenerate eigencharges are observed for some systems, due to the unconstrained geometry relaxation. For the  $O_{48f}$  position, the diagonalization of the symmetric part of the Born tensor gives three non-degenerate eigenvectors, along the  $[011]$ ,  $[100]$  and  $[0\bar{1}1]$  directions (with increasing eigenvalues in the same order). If we consider the plane defined by the B–O–B elements, the first direction corresponds to the  $C_2$  axis, the second is perpendicular to the plane, and the third goes from B to B. Finally, the  $O_{8b}$  tensor is isotropic, and only the diagonal component is given in the table.

The charge for the A site (generally higher than the nominal  $+3e$ , both for the La and Y pyrochlores studied here) is almost independent of the B site composition, with variations smaller than 6%. Similar variations ( $\sim 10\%$ ) are observed for the  $O_{8b}$ . A larger chemical dependence is observed for the dynamical charges associated to the octahedron formed by the B cation and the  $O_{48f}$ . In this case, there are differences in the Born

charges for the B cation of up to 40%, and up to 30% for the  $O_{48f}$ , when the B-site is occupied by Sn instead of Zr or Ti.

The dynamical charges  $Z_B^*$  increase in the order B=Sn, Hf, Zr, Ti. The large anomalous charge contributions (additional charges to the nominal ionic values of  $A^{+3}$ ,  $B^{+4}$  and  $O^{-2}$ ) originate from the electronic charge reorganization induced when an atom is displaced from its original position. They are correlated to charge transfers between atoms and dynamical changes in the hybridization. Large values of Born charges have been observed in Ti-perovskites and attributed to the hybridization between the occupied O  $2p$  orbitals and the unoccupied Ti  $3d$  orbitals.<sup>19</sup> Hence, it would be naive to conclude that the degree of ionicity in pyrochlores increases in the same direction (Sn, Hf, Zr, and Ti) as  $Z_B^*$ .

Figure 2 shows the density of states close to the Fermi level for the four lanthanum structures studied (those for yttrium-pyrochlore are very similar). The valence band has a main contribution from the  $2p$  orbitals of oxygen, and a small contribution from the  $d$  orbitals of the B cation ( $5s$  and  $5p$  orbitals for Sn). The conduction bands

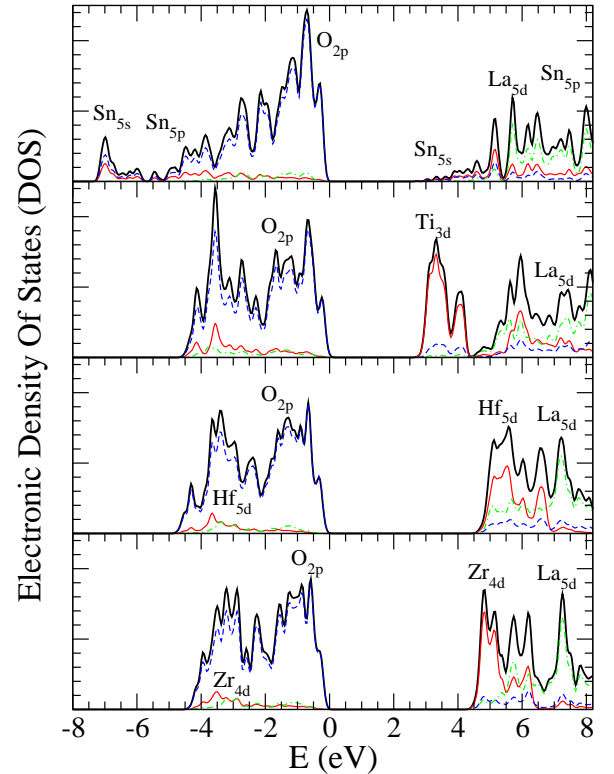


FIG. 2: (Color online) Electronic density of states (DOS) for the  $La_2B_2O_7$  pyrochlores, with B=Sn, Ti, Hf and Zr (from top to bottom panel). The top of the valence band is at 0 eV. The dashed, and dot-dashed lines show the projected contribution into the  $O_{2p}$  and  $La_{5d}$  atomic orbitals. The thin solid line shows the projection into the Sn  $5s$  and  $5p$  orbitals, the Ti  $3d$ , Zr  $4d$ , and Hf  $5d$ , for each system.

TABLE III: Calculated dynamical effective charge tensors for the A ion centered at  $(\frac{1}{2}, \frac{1}{2}, \frac{1}{2})$ , B ion at position  $(0, 0, 0)$ ,  $O_{48f}$  ion at  $(x, \frac{1}{8}, \frac{1}{8})$ , and  $O_{8b}$  ion at  $(\frac{3}{8}, \frac{3}{8}, \frac{3}{8})$ . The effective charge tensor for any other atom can be obtained applying the symmetry operations of the crystal. The eigenvalues of the symmetric part of the tensor are also given.

	$Z_A^*$	$Z_B^*$	$Z_{O_{48f}}^*$	$Z_{O_{8b}}^*$
$La_2Sn_2O_7$	$\begin{pmatrix} 4.12 & 0.19 & 0.19 \\ 0.19 & 4.12 & 0.19 \\ 0.19 & 0.19 & 4.12 \end{pmatrix}$ [3.93, 3.93, 4.50]	$\begin{pmatrix} 4.19 & -0.19 & -0.19 \\ -0.19 & 4.19 & -0.19 \\ -0.19 & -0.19 & 4.19 \end{pmatrix}$ [4.38, 4.38, 3.81]	$\begin{pmatrix} -2.24 & 0.00 & 0.00 \\ 0.00 & -2.31 & 0.24 \\ 0.00 & 0.24 & -2.31 \end{pmatrix}$ [-2.07, -2.24, -2.55]	-2.88
$La_2Hf_2O_7$	$\begin{pmatrix} 4.09 & 0.23 & 0.23 \\ 0.23 & 4.09 & 0.23 \\ 0.23 & 0.23 & 4.09 \end{pmatrix}$ [3.86, 3.86, 4.55]	$\begin{pmatrix} 5.69 & -0.40 & -0.40 \\ -0.40 & 5.69 & -0.40 \\ -0.40 & -0.40 & 5.69 \end{pmatrix}$ [6.09, 6.09, 4.89]	$\begin{pmatrix} -2.55 & 0.00 & 0.00 \\ 0.00 & -2.90 & 0.76 \\ 0.00 & 0.76 & -2.90 \end{pmatrix}$ [-2.14, -2.55, -3.66]	-2.88
$La_2Zr_2O_7$	$\begin{pmatrix} 4.11 & 0.20 & 0.20 \\ 0.20 & 4.11 & 0.20 \\ 0.20 & 0.20 & 4.11 \end{pmatrix}$ [3.91, 3.91, 4.55]	$\begin{pmatrix} 6.00 & -0.37 & -0.37 \\ -0.37 & 6.00 & -0.37 \\ -0.37 & -0.37 & 6.00 \end{pmatrix}$ [6.46, 6.46, 5.35]	$\begin{pmatrix} -2.55 & 0.00 & 0.00 \\ 0.00 & -3.07 & 1.06 \\ 0.00 & 1.06 & -3.07 \end{pmatrix}$ [-2.01, -2.55, -4.13]	-2.89
$La_2Ti_2O_7$	$\begin{pmatrix} 4.20 & 0.20 & 0.20 \\ 0.20 & 4.20 & 0.20 \\ 0.20 & 0.20 & 4.20 \end{pmatrix}$ [4.00, 4.00, 4.60]	$\begin{pmatrix} 6.91 & 0.01 & 0.01 \\ 0.02 & 6.90 & 0.01 \\ 0.02 & 0.01 & 6.90 \end{pmatrix}$ [6.89, 6.89, 6.93]	$\begin{pmatrix} -2.57 & 0.00 & 0.00 \\ 0.00 & -3.53 & 1.56 \\ 0.00 & 1.56 & -3.53 \end{pmatrix}$ [-1.97, -2.57, -5.09]	-2.99
$Y_2Sn_2O_7$	$\begin{pmatrix} 3.93 & 0.06 & 0.06 \\ 0.06 & 3.93 & 0.06 \\ 0.06 & 0.06 & 3.91 \end{pmatrix}$ [3.86, 3.87, 4.04]	$\begin{pmatrix} 4.06 & -0.18 & -0.18 \\ -0.18 & 4.07 & -0.18 \\ -0.18 & -0.18 & 4.06 \end{pmatrix}$ [4.24, 4.24, 3.70]	$\begin{pmatrix} -2.15 & 0.00 & 0.00 \\ 0.00 & -2.24 & 0.18 \\ 0.00 & 0.18 & -2.24 \end{pmatrix}$ [-2.06, -2.15, -2.42]	-2.69
$Y_2Hf_2O_7$	$\begin{pmatrix} 3.90 & 0.07 & 0.07 \\ 0.07 & 3.90 & 0.07 \\ 0.07 & 0.07 & 3.90 \end{pmatrix}$ [3.83, 3.83, 4.04]	$\begin{pmatrix} 5.67 & -0.45 & -0.45 \\ -0.45 & 5.67 & -0.45 \\ -0.45 & -0.45 & 5.67 \end{pmatrix}$ [6.12, 6.12, 4.77]	$\begin{pmatrix} -2.55 & 0.00 & 0.00 \\ 0.00 & -2.84 & 0.74 \\ 0.00 & 0.74 & -2.84 \end{pmatrix}$ [-2.10, -2.55, -3.58]	-2.68
$Y_2Zr_2O_7$	$\begin{pmatrix} 3.94 & 0.04 & 0.04 \\ 0.04 & 3.94 & 0.04 \\ 0.04 & 0.04 & 3.94 \end{pmatrix}$ [3.90, 3.90, 4.02]	$\begin{pmatrix} 5.98 & -0.46 & -0.43 \\ -0.46 & 5.98 & -0.43 \\ -0.43 & -0.43 & 5.98 \end{pmatrix}$ [6.40, 6.44, 5.10]	$\begin{pmatrix} -2.55 & 0.00 & 0.00 \\ 0.00 & -3.01 & 1.03 \\ 0.00 & 1.03 & -3.01 \end{pmatrix}$ [-2.00, -2.55, -4.02]	-2.70
$Y_2Ti_2O_7$	$\begin{pmatrix} 3.96 & 0.03 & 0.03 \\ 0.03 & 3.96 & 0.03 \\ 0.03 & 0.03 & 3.96 \end{pmatrix}$ [3.93, 3.93, 4.02]	$\begin{pmatrix} 6.89 & -0.16 & -0.16 \\ -0.16 & 6.89 & -0.16 \\ -0.16 & -0.16 & 6.89 \end{pmatrix}$ [7.05, 7.05, 6.57]	$\begin{pmatrix} -2.57 & 0.00 & 0.00 \\ 0.01 & -3.46 & 1.50 \\ 0.01 & 1.50 & -3.46 \end{pmatrix}$ [-1.96, -2.57, -4.96]	-2.73

have a sharp peak with B cation  $d$  orbital character in its lower part, and contributions from the  $5d$  orbitals of the La atom.  $La_2Sn_2O_7$  has a very dispersive conduction band with tin- $5s$  character. The anomalous contributions for the B cations can be interpreted as a result of electron current flowing from the occupied  $O_{2p}$  states into the empty states of the B-cation in the conduction band when the B ion is displaced from its equilibrium position. The calculated band gaps are 2.6, 2.8, 4.7 and 4.5 eV for Sn, Ti, Hf, and Zr respectively. The LDA band gaps are known to be underestimated, and a correction of the strong correlation effects is likely to increase the band gap and reduce the Born effective charges<sup>34</sup>.

## B. Static charges

Many definitions of atomic static charges can be found in the literature. They differ in the way the space is partitioned and the charge is associated to each atom. Probably the most popular method is the Mulliken population analysis<sup>35</sup>, where the atomic basis functions are used to associate the electronic density around each atom. Unfortunately, it is well known that the atomic charges obtained with this method are basis-dependent. Recently, Fonseca-Guerra *et al.* showed that the Voronoi Deformation Density (VDD) method give chemically meaningful charges with basis set independency<sup>36</sup>. This method is based in direct integration of the deformation density  $\delta\rho(r) = \rho(r) - \rho_{atom}(r)$  over the Voronoi polyhe-

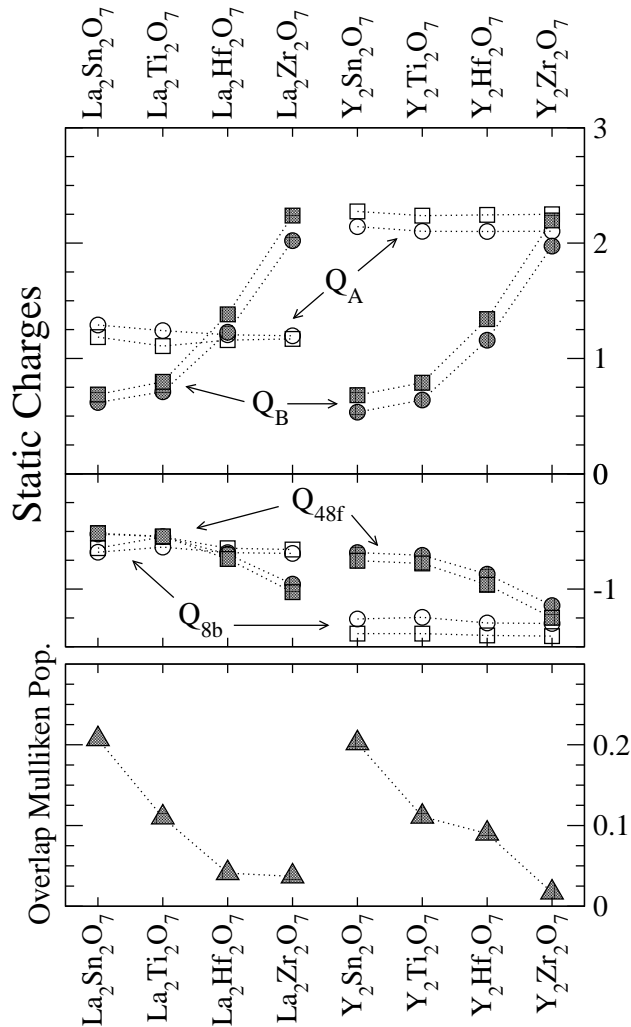


FIG. 3: Static charges calculated with VDD (squares) and Hirshfeld (circles) methods. Upper panel: the cationic charges for the A and B sites (empty and filled symbols). Middle panel: oxygen 48f (filled) and 8b charges (empty). Lower panel: Overlap Mulliken populations between B and  $O_{48f}$  for the two families studied.

dron around each atom. The charges obtained with VDD are similar to the values obtained with the Hirshfeld method<sup>37</sup>, where the electron density is assigned to each atom by weighting with the isolated atom density  $\rho_{atom}(r)$ .

In Fig.3 we show the calculated static charges with VDD and Hirshfeld methods for the cations A and B, and for the two anion sites 8b and 48f. We observe that the values of Hirshfeld and Voronoi charges are very similar. The composition of the A site affects slightly the values for other atoms, specially for the  $O_{8b}$ . This is because the 8b oxygens are surrounded by just four A cations, and no B cation is close enough. The most im-

portant dependence on the chemical composition appears in the charge of the cation B site, with increasing values in the order Sn, Ti, Hf and Zr. If the degree of ionicity of the pyrochlores is to be associated to the static atomic charges this very ordering would be the order of increasing ionicity (larger atomic charge). Notice that the  $O_{48f}$  anions also accumulate more negative charge as we move from Sn to Zr, showing that the  $B-O_{48f}$  pairs become more ionic. To further validate this assignment, we also show the *overlap Mulliken population* between the oxygen atoms and the atoms in the A and B sites<sup>38</sup> (lower panel). These values, though basis-dependent, can be used to estimate the degree of covalency (the larger the overlap, the larger the covalency). It is shown that the overlap population of the oxygen decreases in the order  $Sn > Ti > Hf > Zr$ .

### C. Charge distribution

Figure 4 plots the contour of electronic charge redistribution  $\delta\rho(r)$  in a plane defined by A-B- $O_{48f}$ , for  $Y_2Ti_2O_7$ ,  $Y_2Hf_2O_7$ , and  $Y_2Zr_2O_7$ . The valence configuration for Ti, Hf and Zr is similar, as well as the lattice structure. Consequently, the differences in the contour plots have to be attributed to the difference bonding character with oxygen in the three systems. The stannate is not included here, because of the different valence configuration of Sn. The directional character of the Ti-O bond is in contrast with the mainly ionic Zr-O. The hafnate presents an intermediate directionality. Similar contour plots are observed for the lanthanides. Notice that the charge distribution around the A site is mainly spherical showing the high ionicity. The contour plots support the hypothesis of increasing covalency from Ti to Hf to Zr based pyrochlores.

## IV. DISCUSSION

Understanding response of materials to radiation is a very complex problem. Many factors have been named to be relevant in the context of resistance to amorphization by irradiation<sup>15</sup>, including topological freedom, glass-forming ability, melting and crystallization temperatures, ionicity, bond energy, elasticity, ratio of ionic radii, defect formation energies, etc. Many criteria to characterize radiation resistance focus in a particular subset of properties. In pyrochlores, the defect-formation energies have been a popular criterion. It was thought that the ionic radius or ionic radius ratio were the most important factors in determining the defect energies,<sup>5</sup> but recent first-principles calculations have demonstrated that the electronic structure plays an important role.<sup>11</sup> The fact that all pyrochlores have the same structure, makes them an excellent playground to tests the relevance of some of these factors, and particularly the role of the bond-type.

Naguib and Kelly proposed a criterion for resistance



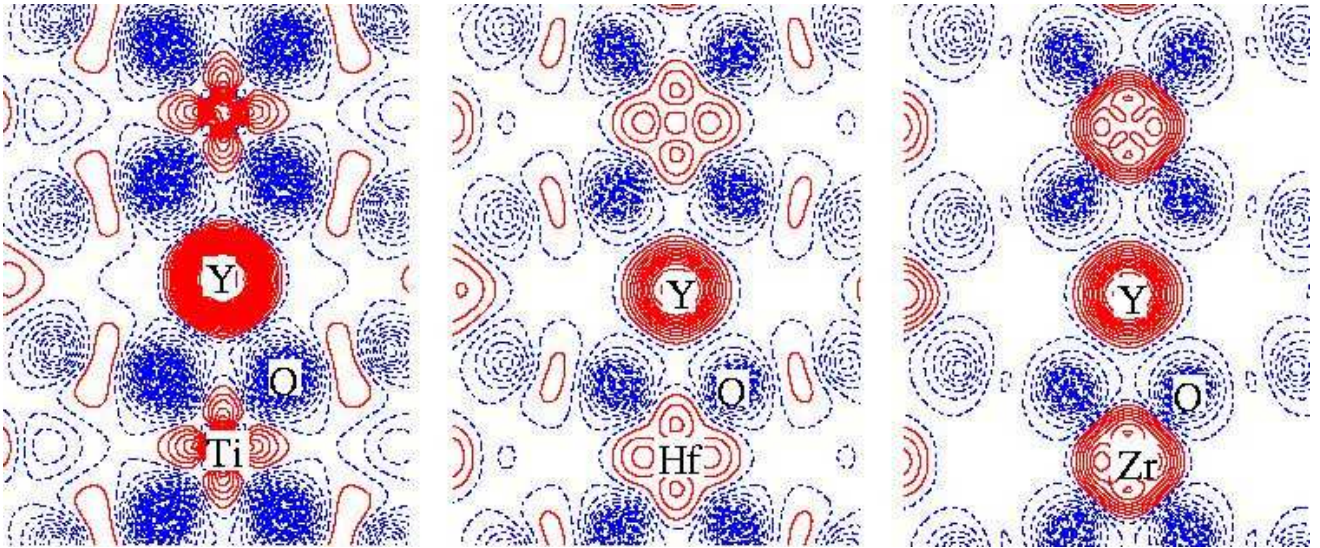


FIG. 4: (Color online) Electronic charge redistribution in the A-B-O<sub>48f</sub> plane. The lines are taken at intervals of 0.005e in the range -0.25e to 0.25e. Solid (red) and dashed (blue) lines correspond to positive and negative values respectively.

to amorphization by irradiation based on the good empirical correlation between ionicity and susceptibility to amorphization<sup>39</sup>. Frequently, the ionicity of the material is quantified from the difference in Pauling or Phillips electro-negativities for different atoms resulting in inconsistencies of the Naguib and Kelly criterion. Nevertheless, the importance of ionicity/covalency in the radiation resistance is evident. For the family of pyrochlores studied here, the static atomic charges, and overlap Mulliken populations indicate that ionicity increases as the B site is occupied by Sn, Ti, Hf and Zr. Remarkably, this is consistent with the increase of resistance of these materials. The critical temperature ( $T_c$ ) above which complete amorphization of the material can not be obtained is frequently used as a measure of the resistance to amorphization of the material. The lower  $T_c$ , the more resistant the material. For the family of lanthanide pyrochlores La<sub>2</sub>Sn<sub>2</sub>O<sub>7</sub> (1025 K), La<sub>2</sub>Hf<sub>2</sub>O<sub>7</sub> (563 K) and La<sub>2</sub>Zr<sub>2</sub>O<sub>7</sub> (339 K), the trend agrees with the decrease of covalency, and with the Naguib and Kelly criterion. Furthermore, the observed<sup>40</sup> increase in resistance to amorphization with increasing zirconium content in Gd<sub>2</sub>Ti<sub>2-x</sub>Zr<sub>x</sub>O<sub>7</sub> seems to follow the same trend. However, Y<sub>2</sub>Sn<sub>2</sub>O<sub>7</sub> with a critical temperature similar to the one observed for the hafnate, deviates from this trend and would require further study.

The deformation density contour plot for A<sub>2</sub>Ti<sub>2</sub>O<sub>7</sub> indicates that these pyrochlores have an important covalent character, as opposed to A<sub>2</sub>Hf<sub>2</sub>O<sub>7</sub> and A<sub>2</sub>Zr<sub>2</sub>O<sub>7</sub> where a more ionic character can be deduced from the deformation density. The nearly identical defect formation energies calculated for the Ti and Sn members in reference [11] could be a consequence of the similar covalent bond. We believe that the highly anomalous Born charge calculated for Ti has an origin on the hybridization between the 2p orbitals of oxygen and the 3d orbitals of Ti, simi-

larly to the anomalous Born charges observed for example in Ti-perovskites, or TiO<sub>2</sub>, and should not be attributed to a strongly ionic character of these pyrochlores.

The calculated elastic constants do not satisfy the Cauchy relation  $c_{12}/c_{44} = 1$ . This condition has to be satisfied in crystals with two-body interactions, as in a purely ionic system. In particular, for La<sub>2</sub>Sn<sub>2</sub>O<sub>7</sub>, La<sub>2</sub>Hf<sub>2</sub>O<sub>7</sub>, Y<sub>2</sub>Ti<sub>2</sub>O<sub>7</sub> and Y<sub>2</sub>Sn<sub>2</sub>O<sub>7</sub> we have  $c_{12}/c_{44} < 0.75$ . The presence of non-central forces, such as those coming from covalent bonding produces deviations from Cauchy equality. The relation is more strongly broken for the unrelaxed elastic constants ( $c_{12}^0/c_{44}^0$ ), and is partially recovered under relaxation. The surprising recovery observed for La<sub>2</sub>Ti<sub>2</sub>O<sub>7</sub> could be related to the instability of the pyrochlore structure for this system.

## V. CONCLUSIONS

In this work we have used density functional theory calculations to analyze the structural and chemical properties of a family of pyrochlores. The lattice and structural parameters ( $a$  and  $x$ ) were obtained with a conjugate gradient minimization of the forces and strains. Applying a particular set of lattice distortions, the elastic constants were also obtained. The structural properties obtained from first principles can be used to parametrize new interatomic potentials that could be used in classical Molecular Dynamics simulations for materials design. The lack of an accurate description of the chemical bond in these classical simulations was criticized recently in the context of resistance to amorphization by irradiation.

Although experimental evidence shows that the electronic structure has to play some role in radiation resistance, it is still not clear what is the trend. The similar

lattice structure for the ideal systems (not all of them stable in the pyrochlore structure) studied here, makes them excellent systems to elucidate the relevance of the chemical properties. If the description of Trachenko and collaborators is correct, the competition between short (covalent) and long (ionic) interactions is strongly related to the resistance to amorphization<sup>15,16</sup>.

In this work we present a study of some indicators of covalency/ionicity in pyrochlores. Although some of these parameters (static charges, deformation density) seem to show evidence that the stannates and titanates pyrochlores have a more covalent character than the highly ionic hafnates and zirconates, (which are known to be more resistant to amorphization), others, like the dynamical charges, do not show the same trend. Fur-

ther work is required to understand these differences. In particular, a systematic experimental study of  $T_c$  is desirable, as most of the available data is recorded in different conditions (bombarding ions, energy, etc.).

### Acknowledgments

This work was supported by BNFL and UK's NERC through the eminerals consortium. The authors are grateful to G. Lumpkin, K. Whittle, K. Trachenko, I. Farnan, and S. Ríos for fruitful discussions on radiation resistance of pyrochlores. EA thanks the Donostia International Physics Center (DIPC) for its hospitality.

- <sup>1</sup> D. P. Cann, C. A. Randall, and T. R. Shrout, Solid State Commun. **100**, 529 (1996); T. R. Shrout and S. L. Swartz, Mater. Res. Bull. **18**, 663 (1983).
- <sup>2</sup> R. Vassen, X. Cao, F. Tietz, D. Basu, and D. Stöver, J. Am. Ceram. Soc. **83**, 2023 (2000); G. Suresh, G. Seenivasan, M. V. Krishnaiah, and P. S. Murti, J. Nucl. Mater. **249**, 259 (1997).
- <sup>3</sup> B. J. Wuensch, K. W. Eberman, C. Heremans, E. M. Ku, P. Omnerud, E. M. E. Yeo, S. M. Haile, J. K. Stalick, and J. D. Jorgensen, Solid State Ionics. **129**, 111 (2000).
- <sup>4</sup> R. C. Ewing, W. J. Weber, and J. Lian, J. Appl. Phys. **95**, 5949 (2004).
- <sup>5</sup> K. E. Sickafus, L. Minervini, R. W. Grimes, J. A. Valdez, M. Ishimaru, F. Li, K. J. McClellan, T. Hartmann, Science **289**, 748 (2000).
- <sup>6</sup> P. K. Schelling, S. R. Phillpot, and R. W. Grimes, Phil. Mag. Lett. **84**, 127 (2004).
- <sup>7</sup> Y. Tabira, R. L. Withers, L. Minervini, and R. W. Grimes, J. Solid State Chem. **153**, 16 (2000).
- <sup>8</sup> G. R. Lumpkin, K. R. Whittle, S. Rios, K. L. Smith, and N. J. Zaluzec, J. Phys.: Condens. Matter. **16**, 8557 (2004).
- <sup>9</sup> M. Pirzada, R. W. Grimes, L. Minervini, J. F. Maguire, and K. E. Sickafus, Solid State Ionics **140**, 201 (2001).
- <sup>10</sup> A. Chartier, C. Meis, W. J. Weber, and L. R. Corrales, Phys. Rev. B **65**, 134116 (2002).
- <sup>11</sup> Wendy R. Panero, Lars Stixrude, and Rodney C. Ewing, Phys. Rev. B **70**, 054110 (2004).
- <sup>12</sup> J. Lian, R. C. Ewing, L. M. Wang, and K. B. Helean, J. Mater. Res. **19**, 1575 (2004).
- <sup>13</sup> J. Lian, J. Chen, L. M. Wang, R. C. Ewing, J. M. Farmer, L. A. Boatner, and K. B. Helean, Phys. Rev. B **68**, 134107 (2004).
- <sup>14</sup> K. Trachenko, M. Pruneda, E. Artacho, M. T. Dove, Phys. Rev. B **70**, 134112 (2004).
- <sup>15</sup> K. Trachenko, J. Phys.: Cond. Matt. **16**, R1491 (2004).
- <sup>16</sup> K. Trachenko, J. M. Pruneda, E. Artacho, and M. T. Dove, Phys. Rev. B **71**, 184104 (2005).
- <sup>17</sup> L. W. Hobbs, Nucl. Instrum. Methods B **91**, 30 (1994).
- <sup>18</sup> Not all the compounds in the families studied are stable in the pyrochlore structure. For example  $\text{La}_2\text{Ti}_2\text{O}_7$  has the layered perovskite structure.
- <sup>19</sup> Ph. Ghosez, J. -P. Michenaud, and X. Gonze, Phys. Rev. B **58**, 6224 (1998).
- <sup>20</sup> M. A. Subramanian, G. Aravamudan, G. V. S. Rao, Prog. Solid. State Chem. **15**, 55 (1983).
- <sup>21</sup> P. Ordejón, E. Artacho, and J. M. Soler, Phys. Rev. B **53**, R10441 (1996); J. M. Soler, E. Artacho, J. D. Gale, A. García, J. Junquera, P. Ordejón and D. Sánchez-Portal, J. Phys.: Condens. Matter **14**, 2745 (2002).
- <sup>22</sup> P. Hohenberg and W. Kohn, Phys. Rev. **136**, B864 (1964); W. Kohn and L. J. Sham, Phys. Rev. **140**, A1133 (1965).
- <sup>23</sup> D. M. Ceperley and B. J. Alder, Phys. Rev. Lett. **45**, 566 (1980).
- <sup>24</sup> N. Troullier and J. L. Martins, Phys. Rev. B **43**, 1993 (1991).
- <sup>25</sup> L. Kleinman and D.M. Bylander, Phys. Rev. Lett. **48**, 1425 (1982).
- <sup>26</sup> S. G. Louie, S. Froyen, M. L. Cohen, Phys. Rev. B **26**, 1738 (1982).
- <sup>27</sup> B. J. Kennedy, B. A. Hunter, and C. J. Howard, J. Solid State Chem. **130**, 58 (1997).
- <sup>28</sup> L. Minervini, R. W. Grimes, Y. Tabira, R. L. Withers, K. E. Sickafus, Philos. Mag. **82**, 123 (2002).
- <sup>29</sup> O. H. Nielsen and R. M. Martin, Phys. Rev. Lett. **50**, 697 (1983).
- <sup>30</sup> R. Stadler, W. Wolf, R. Podloucky, G. Kresse, J. Furthmüller, and J. Hafner, Phys. Rev. B **54**, 1729 (1996).
- <sup>31</sup> H. Ibach and H. Lüth *Solid-State Physics. An introduction to Principles of Materials Science* (Springer-Verlag, Berlin (1996).
- <sup>32</sup> R. A. Robie and J. L. Edwards, J. Appl. Phys. **37**, 2659 (1966).
- <sup>33</sup> M. Posternak, R. Resta, and A. Baldereschi, Phys. Rev. B **50**, R8911 (1994).
- <sup>34</sup> A. Filippetti and N. A. Spaldin, Phys. Rev. B **68**, 045111 (2003).
- <sup>35</sup> R. S. Mulliken, J. Chem. Phys. **23**, 1833 (1955).
- <sup>36</sup> C. Fonseca Guerra, J.-W. Handgraaf, E. J. Baerends, F. M. Bickelhaupt, J. Comput. Chem. **25**, 189 (2003).
- <sup>37</sup> F. L. Hirshfeld, Theoret. Chim. Acta **44** 129 (1977).
- <sup>38</sup> G. R. Lumpkin, S. Ríos, K. R. Whittle, J. M. Pruneda, K. Trachenko, K. L. Smith, and N. J. Zaluzec, *to be published*.
- <sup>39</sup> H. N. Naguib and R. Kelly, Radiat. Eff. **25**, 1 (1975).
- <sup>40</sup> S. X. Wang, B. D. Begg, L. M. Wang, R. C. Ewing, W. J. Weber, and K. V. Kuty, J. Mater. Res. **14**, 4470 (1999).